SUPERSONIC VISCOUS GAS FLOW AROUND A COOLED SPHERICAL BLUNT BODY

Yu. P. Golovachev and F. D. Popov

UDC 533.6.011.55::533.16

An investigation is made of the supersonic flow around a spherical blunt body on the basis of equations obtained from the Navier–Stokes equations without taking into account terms of order $O(R^{-1/2})$, $O(R^{-1})$, etc., throughout the shock layer (R is the Reynolds number). The equations used are applicable for arbitrary values of the ratio of densities at the shock wave, which is taken here to be a surface of discontinuity. A comparison of the results of our calculations with known solutions of the complete Navier–Stokes equations, with results obtained from the theory of nonviscous flow and also from boundary layer theory, and also with experimental data show that our formulation of the problem is valid for Reynolds numbers $R_\infty \geqslant 10^2$. In the range $10^2 \leqslant R_\infty \leq 10^5$ we investigate the change of aerodynamic characteristics of the cooled blunt body and the parameters of the shock layer as a function of the Reynolds number and the temperature factor for moderate supersonic speeds of the incident flow.

1. In estimating the terms of the complete Navier–Stokes equations it is assumed that the thickness of the region adjacent to a wall, a region in which the viscosity and thermal conductivity of the gas play a substantial role, and also the magnitude of the velocity component normal to the body surface in this region are of order $O(R^{-1/2})$. If we take into account only terms of order O(1) in some part of the shock layer, we obtain a system of equations which includes all the terms of the equations of nonviscous flow and also those of the boundary layer flow. In spherical coordinates, for the axially symmetric nonstationary case, this system of equations has the form

$$\begin{gathered}
\frac{\partial h}{\partial t}+u\frac{\partial h}{\partial r}+\frac{v}{r}\frac{\partial h}{\partial \theta}=\frac{2}{\rho}\left[\frac{\partial p}{\partial t}+u\frac{\partial p}{\partial r}+\frac{v}{r}\frac{\partial p}{\partial \theta}+\frac{\mu}{R}\left(\frac{\partial v}{\partial r}\right)^2+\frac{1}{RP}\frac{\partial}{\partial r}\left(\lambda\frac{\partial T}{\partial r}\right)\right]\\
\frac{\partial v}{\partial t}+u\frac{\partial v}{\partial r}+\frac{v}{r}\frac{\partial v}{\partial \theta}+\frac{uv}{r}=-\frac{1}{\rho r}\frac{\partial p}{\partial \theta}+\frac{1}{\rho R}\frac{\partial}{\partial r}\left(\mu\frac{\partial v}{\partial r}\right)\\
\frac{\partial u}{\partial t}+u\frac{\partial u}{\partial r}+\frac{v}{r}\frac{\partial u}{\partial \theta}-\frac{v^2}{r}=-\frac{1}{\rho}\frac{\partial p}{\partial r}\\
\frac{\partial \rho}{\partial t}+u\frac{\partial \rho}{\partial r}+\frac{v}{r}\frac{\partial \rho}{\partial \theta}+\frac{\rho}{r}\left(r\frac{\partial u}{\partial r}+\frac{\partial v}{\partial \theta}+2u+v\operatorname{ctg}\theta\right)=0\\
h=h(\rho, T), \qquad p=p(\rho, T), \qquad \mu=\mu(T), \qquad \lambda=\lambda(T)
\end{gathered} \tag{1.1}$$

Here the velocity components u, v (along the r and θ axes, respectively) are referred to the maximum velocity V, the density ρ is referred to the density in the incident flow ρ_∞, the pressure p to $\rho_\infty V^2$, the temperature T to $m_\infty V^2/R^*$ (m_∞ is the molecular weight of the gas in the incident flow, and R* is the universal gas constant), the specific enthalpy h is referred to $\frac{1}{2}V^2$, the linear dimensions are referred to the bluntness radius a, the time t to a/V, the coefficients of viscosity μ and thermal conductivity λ are referred to corresponding values μ^* and λ^* calculated at the temperature $T = m_\infty V^2/R^*$. The Reynolds and Prandtl numbers are defined as follows:

$$R=\frac{V\rho_\infty a}{\mu^*}, \qquad P=\frac{\mu^* R^*}{\lambda^* m_\infty}$$

We solve Eqs. (1.1) in a region bounded by the surface of the body, the axis of symmetry $\theta = 0$, the shock wave, which is taken to be a discontinuity surface, and some ray $\theta^* > 0$. The boundary conditions of the problem are formulated as follows. On the body surface we pose the usual conditions of nonpentrability and nonslippage for the velocity components and the temperature condition $T = T_W = \text{const}$, on the $\theta = 0$ axis

Leningrad. Translated from Zhurnal Prikladnoi Mekhaniki i Tekhnicheskoi Fiziki, No. 5, pp. 135–142, September–October, 1972. Original article submitted April 17, 1972.

we have conditions of symmetry, and at the shock wave we use the nonstationary Rankine–Hugoniot relations [1]. No additional conditions are posed on the boundary ray $\theta = \theta^*$ since it was shown in [2] that for θ^* sufficiently large the reverse flow effect on the flow in the region considered is small. In most of our calculations we used $\theta^* = 90°$

2. For the solution of the problem it is convenient to introduce new independent spatial variables x, y:

$$x = \frac{\ln(1+H\xi)}{\ln(1+H)}, \quad y = \theta \quad \left(\xi = \frac{r - G(\theta)}{F(\theta, t) - G(\theta)}, \quad H > 0\right) \tag{2.1}$$

where $r = G(\theta)$ and $r = F(\theta, t)$ are the equations of the body contour and the shock wave. In the variables (2.1) the flow region considered becomes rectangular and the curves $\xi = \text{const}$ are concentrated at the body surface as the parameter H increases. In matrix form the initial system of Eqs. (1.1) may be described as follows:

$$\begin{gathered} \mathbf{E}\frac{\partial \mathbf{X}}{\partial t} + \mathbf{A}\frac{\partial^2 \mathbf{X}}{\partial x^2} + \mathbf{B}\frac{\partial \mathbf{X}}{\partial x} + \mathbf{C}\frac{\partial \mathbf{X}}{\partial y} + \mathbf{D} = 0 \\ \mathbf{e}\frac{\partial \mathbf{X}}{\partial t} + \mathbf{b}\frac{\partial \mathbf{X}}{\partial x} + \mathbf{c}\frac{\partial \mathbf{X}}{\partial y} + \mathbf{d} = 0 \end{gathered} \tag{2.2}$$

where $\mathbf{X} = \{Tvu\rho\}'$ is a column vector of the unknown quantities and the rectangular matrices **E**, **A**, **B**, **C**, **D**, **e**, **b**, **c**, **d** are defined in terms of the coefficients of the system of Eqs. (1.1).

In the region $0 \le x \le 1$, $0 \le y \le \theta^*$, $t \ge 0$ we introduce a computational mesh with the nodal coordinates

$$\begin{gathered} x_i = ih \quad (h = 1/M, \quad i = 0, 1, \ldots, M), \qquad y_j = jl \quad (l = \theta^*/N, \quad j = 0, 1, \ldots, N) \\ t^n = n\Delta t \quad (n = 0, 1, 2, \ldots) \end{gathered} \tag{2.3}$$

The system of differential equations (2.2) is replaced by a system of difference equations with the use of an implicit (with weight α) scheme having second order approximation in the spatial variables. The coefficients of the system are described at a point "suspended" between the layers n and n+1. The boundary-value problem for the resulting nonlinear system of difference equations is solved by the method of successive approximations, similar to that given in [1] for calculating nonviscous gas flows. To determine the vector of the unknown functions at the (n+1)-th layer in (s+1) iterations from the known data at the n-th layer, we consider the coefficients of the system and also the derivatives with respect to y as known from the previous s iterations.

Then the complete system of difference equations breaks up into independent subsystems of the form (2.4) and (2.5) for the unknowns on the separate rays $y = y_j$:

$$\mathbf{P}_i^{n+(\alpha s)}\mathbf{X}_{i+1}^{n+(s+1)} + \mathbf{R}_i^{n+(\alpha s)}\mathbf{X}_i^{n+(s+1)} + \mathbf{Q}_i^{n+(\alpha s)}\mathbf{X}_{i-1}^{n+(s+1)} + \Phi_i^{n+(\alpha s)} = 0 \quad (i = 1, 2, \ldots, M-1) \tag{2.4}$$

$$\mathbf{r}_{i-1/2}^{n+(\alpha s)}\mathbf{X}_i^{n+(s+1)} + \mathbf{q}_{i-1/2}^{n+(\alpha s)}\mathbf{X}_{i-1}^{n+(s+1)} + \varphi_{i-1/2}^{n+(\alpha s)} = 0 \quad (i = 1, 2, \ldots, M) \tag{2.5}$$

where

$$\mathbf{P}_i = \varkappa(2/h\mathbf{A} + \mathbf{B})_i, \quad \mathbf{R}_i = 4(\mathbf{E} - \varkappa/h\mathbf{A}_i), \quad \mathbf{Q}_i = \varkappa(2/h\mathbf{A} - \mathbf{B})_i$$

$$\Phi_i = \frac{1-\alpha}{\alpha}\mathbf{P}_i\mathbf{X}_{i+1}^n + \frac{1}{\alpha}[-4\mathbf{E} + (1-\alpha)\mathbf{R}_i]\mathbf{X}_i^n + \frac{1-\alpha}{\alpha}\mathbf{Q}_i\mathbf{X}_{i-1}^n + 4\Delta t\left(\mathbf{C}\frac{\partial \mathbf{X}}{\partial y} + \mathbf{D}\right)_i$$

$$\mathbf{r}_{i-1/2} = \mathbf{e} + \varkappa\mathbf{b}_{i-1/2}, \quad \mathbf{q}_{i-1/2} = \mathbf{e} - \varkappa\mathbf{b}_{i-1/2} \quad \left(\varkappa = \frac{2\Delta t\alpha}{h}\right);$$

$$\varphi_{i-1/2} = \frac{1}{\alpha}[-\mathbf{e} + (1-\alpha)\mathbf{r}_{i-1/2}]\mathbf{X}_i^n + \frac{1}{\alpha}[-\mathbf{e} + (1-\alpha)\mathbf{q}_{i-1/2}]\mathbf{X}_{i-1}^n + 2\Delta t\left(\mathbf{c}\frac{\partial \mathbf{X}}{\partial y} + \mathbf{d}\right)_{i-1/2}$$

[we omit the superscript $n + (\alpha s)$ for brevity].

We solve the system of Eqs. (2.4) and (2.5) along each ray by the screw method. Using the boundary conditions on the body for the temperature and the velocity component v, and also both equations of the first order of the Eqs. (2.5) for i = 1, we obtain

$$\mathbf{X}_0 + \Omega_1\mathbf{X}_1 + \Pi_1 = 0 \tag{2.6}$$

where

$$\Omega_1 = \begin{Vmatrix} \mathbf{E} \\ \mathbf{q}_{1/2} \end{Vmatrix}^{-1} \begin{Vmatrix} 0 \\ \mathbf{r}_{1/2} \end{Vmatrix}, \quad \Pi_1 = \begin{Vmatrix} \mathbf{E} \\ \mathbf{q}_{1/2} \end{Vmatrix}^{-1} \begin{Vmatrix} -T_w \\ 0 \\ \varphi_{1/2} \end{Vmatrix}$$

For all i = 1, 2, ... , M we find the relation

$$\mathbf{X}_{i-1} + \Omega_i \mathbf{X}_i + \Pi_i = 0 \tag{2.7}$$

For this we eliminate, with the help of Eq. (2.7), the vector $\mathbf{X_{i-1}}$ from the difference equations of the second order (2.4). Adjoining to the resulting system the first order Eqs. (2.5), we find recursion formulas for determining the coefficients Ω_i, Π_i:

$$\Omega_{i+1} = \begin{Vmatrix} \mathbf{R}_i - \mathbf{Q}_i\Omega_i \\ q_{i+1/2} \end{Vmatrix}^{-1} \begin{Vmatrix} \mathbf{P}_i \\ r_{i+1/2} \end{Vmatrix}, \qquad \Pi_{i+1} = \begin{Vmatrix} \mathbf{R}_i - \mathbf{Q}_i\Omega_i \\ q_{i+1/2} \end{Vmatrix}^{-1} \begin{Vmatrix} \Phi_i - \mathbf{Q}_i\Pi_i \\ \varphi_{i+1/2} \end{Vmatrix} \tag{2.8}$$

We write the as yet unused boundary condition on the body for the normal component u of the velocity in the form

$$\omega_0 \mathbf{X}_0 + \pi_0 = 0 \qquad (\omega_0 = \{0010\}, \quad \pi_0 = 0) \tag{2.9}$$

and we seek a relation of the form (2.9) for all i = 0,1,..., M. Using Eq. (2.7), we readily obtain

$$\omega_{i+1} = \beta\omega_i\Omega_{i+1}, \qquad \pi_{i+1} = \beta(\omega_i\Pi_{i+1} - \pi_i) \tag{2.10}$$

where β is a normalizing factor for which a quantity inverse to the length of the row $\omega_i\Omega_{i+1}$ is chosen. Performing a right rotation, i.e., calculating all the coefficients Ω_i, Π_i, with the aid of Eqs. (2.9) and (2.10) we obtain on the shock wave the relation

$$\omega_M \mathbf{X}_M + \pi_M = 0 \tag{2.11}$$

Adjoining Eq. (2.11) to the nonstationary Rankine–Hugoniot relations and solving the resulting nonlinear system of five equations, we determine the vector of the unknown functions on the shock wave and the quantity F_t', in terms of which the shock wave departure may be determined. The inverse rotation is effected with the aid of the relation (2.7) in which the third equation is replaced by the rotational relation

$$\omega_i \mathbf{X}_i + \pi_i = 0 \tag{2.12}$$

On the axis of symmetry (y = 0), after elimination of the singularity, the system of difference equations for $X = \{Tu\rho\}'$ is solved in an analogous manner. Derivatives with respect to y are calculated at the final ray ($y = \theta^*$) with the aid of nonsymmetric second order difference approximations.

The solution of the problem is regarded as having been attained if, beginning with some time instant, the relative changes in all the functions at an arbitrary node of the mesh decrease for two time layers and if the maximum of these changes proves to be less than $\Delta t \cdot 10^{-3}$.

3. Calculations were made for the case of flow around a sphere by a perfect gas with ratio of specific heat capacities $\gamma = 1.4$ for Reynolds numbers $10^2 \leqslant R_\infty \leq 10^5$. The value of the temperature factor $k = T_w/T_0$ (T_0 is the retardation temperature) was varied over the range from 0.14 to 0.7. It was assumed that the coefficient of dynamic viscosity depends on the temperature according to a power law with exponent ω. In the majority of the calculations we used $\omega = 0.5$ and a Prandtl number $P_\infty = 0.7$. For ease of comparison of the results obtained with existing data in the literature, we used, besides $R_\infty = V_\infty\rho_\infty a/\mu_\infty$, also the quantities

$$R_s = \frac{V_s\rho_s a}{\mu_s} = R_\infty\left[1 + \frac{2(\gamma-1)}{(\gamma+1)^2 M_\infty^2}(M_\infty^2 - 1)(1 + \gamma M_\infty^2)\right]^{-\omega}$$
$$R_w = \frac{2V_\infty\rho_\infty a}{\mu_w} = 2R_\infty(T_\infty/T_w)^\omega \tag{3.1}$$

where the subscript s is used for values of the gas parameters on the axis of symmetry directly back of the shock wave.

The results discussed below ($M_\infty = 6$) were obtained for the following parameter values of the calculational mesh: M = 25, N = 10, H = 100. Control calculations showed, moreover, that an accuracy to within 1% may be ensured over the whole field of the gas-dynamic functions, the shock wave departure, the thermal flow, and the coefficient of friction.

Figure 1 shows how the shock wave departure ε_0 varies on the axis of symmetry as a function of the Reynolds number R_∞. Curves 1, 2, 3, and 4 correspond, respectively, to values of the temperature factor k = 0.7, 0.35, 0.21, 0.14. The dashed curve corresponds to the value of ε_0 obtained from the calculation of a nonviscous gas flow around a sphere (M = 25, N = 10, and a uniform step in the coordinate ξ). It is evident that the temperature factor determines to a significant degree not only the size of the shock wave departure but also the nature of the dependence of ε_0 on the Reynolds number.

In Figs. 2 and 3 we present profiles of the gas-dynamic functions in the shock layer at the $\theta = 45°$ ray for k = 0.35 for $R_\infty = 355$ (curve 1) and 71,000 (curve 2). The dashed curves are the calculated results for

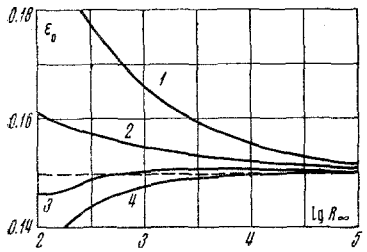

Fig. 1

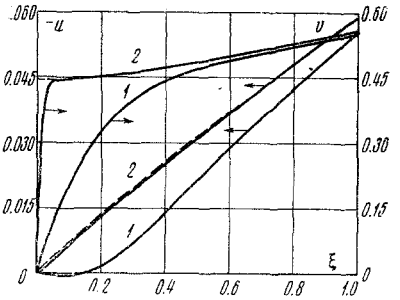

Fig. 2

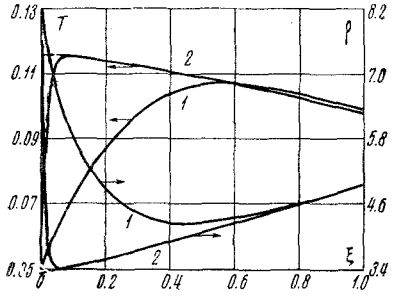

Fig. 3

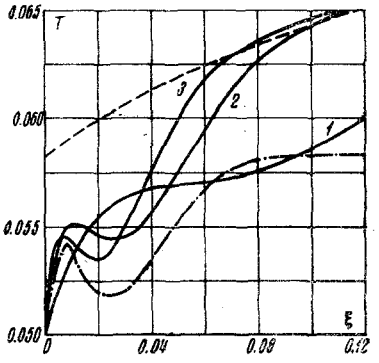

Fig. 4

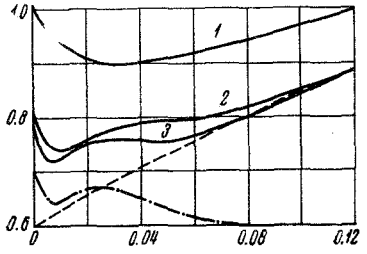

Fig. 5

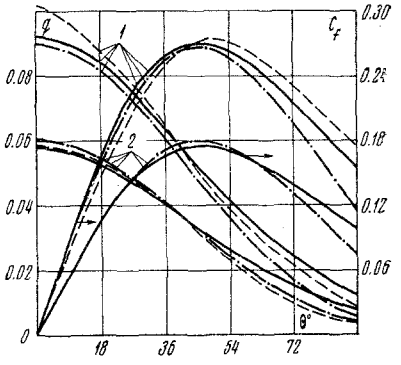

Fig. 6

nonviscous flow. At the shock wave ($\xi = 1$) the values of the gas-dynamic functions do not differ significantly. This indicates that the shock wave shape varies weakly with a change in the Reynolds number. The influence of viscosity and thermal conductivity of the gas becomes apparent in the region at the wall, the size of which decreases with an increase in the Reynolds number. For large θ, with an increase in R_∞ the behavior of the temperature and the density in the region at the wall becomes substantially nonmonotonic.

Figures 4 and 5 show the profiles of T and ρ in this region for $\theta = 90°$ (k = 0.35) for various values of R_∞: curves 1, 2, and 3 are for $R_\infty = 3550$; 35,500; and 71,000, respectively. In these calculations we assumed that $\theta^* = 100°$. The dashed curves represent T and ρ profiles for nonviscous flow while the dash-dot curves give the results for the boundary layer calculation for $R_\infty = 71{,}000$. The boundary layer calculation was made with the aid of a two-layer implicit six-point scheme [3], using at the outer edge of the boundary layer data obtained from solving the nonviscous flow problem. As can be seen from Figs. 4 and 5, for large Reynolds numbers maximum temperatures and minimum densities occur near the body surface, becoming more pronounced and being displaced towards the body as R_∞ increases. We note that for a nonviscous gas the temperature and the density close to the surface vary monotonically (dashed curves). When $\xi \geqslant 0.1$ the T and ρ profiles for $R_\infty = 35{,}500$ and 71,000 are practically coincident with the results of the nonviscous flow calculations. For these values of the coordinate ξ, outflow takes place on the asymptote of the boundary layer solution; however, by virtue of the boundary conditions posed, the asymptotic values of

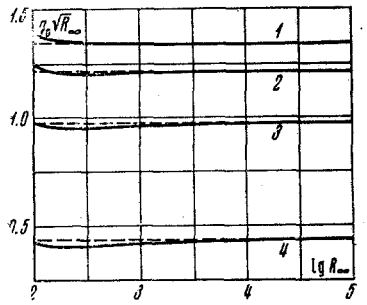

Fig. 7

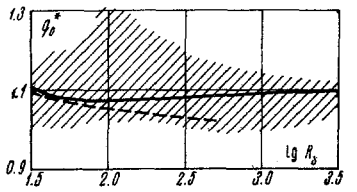

Fig. 8

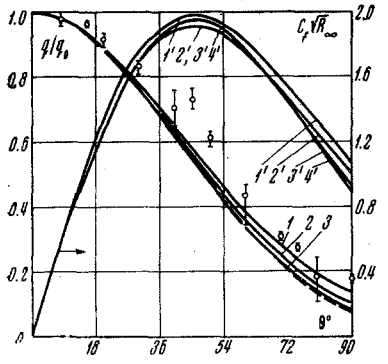

Fig. 9

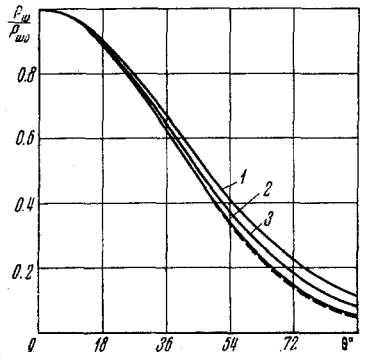

Fig. 10

temperature and density for $\xi \gtrsim 0.1$ differ from the true values of T and ρ, obtained from a calculation of the viscous shock layer. The boundary layer solution yields nonmonotonic temperature and density profiles near the surface as does also the calculation of the viscous shock layer for large Reynolds numbers.

We now proceed to a discussion of the results relating to heat transfer and friction at the body surface. The dimensionless heat flow q and friction coefficient C_f are defined by the formulas

$$q = \frac{1}{\rho_\infty V^3}\left(\lambda \frac{\partial T}{\partial r}\right)'_w, \qquad C_f = \frac{2}{\rho_\infty V^2}\left(\mu \frac{\partial v}{\partial r}\right)'_w \tag{3.2}$$

where the prime indicates dimensional quantities. Figure 6, for $\omega = 3/4$, $P_\infty = 0.72$, $k = 0.527$, gives a comparison of our results (solid curves) with the results obtained in [2] from solving the complete Navier–Stokes equations (dashed curves) and also with the results of the boundary layer calculation (dash-dot curves).

We remark that in [2] no shock wave was assumed at the outer boundary of the flow region and the surface was located entirely in the unperturbed incident flow. Curves 1 correspond to $R_\infty = 90$, curves 2 to $R_\infty = 200$. It is interesting to note that for $\theta \lesssim 60°$ the results of our paper as well as the results given in [2] differ insignificantly from the results calculated according to the classical boundary layer theory, wherein the data used at its outer edge are obtained from the nonviscous flow calculation on the body surface. For large θ the divergence becomes large. It also increases with a decrease in the Reynolds number.

Figure 7 shows the dependence of the quantity $q_0\sqrt{R_\infty}$ on the Reynolds number (q_0 is the dimensionless heat flow at the critical point). The numbers 1, 2, 3, and 4 refer to the results for k = 0.14, 0.21, 0.35, and 0.7. The dashed curves show the corresponding values obtained from solving the boundary layer equations. It is evident that with an increase in the surface temperature the difference of $q_0\sqrt{R_\infty}$ from its boundary layer value occurs for large Reynolds numbers.

For small R_∞, for all values of the temperature factor, the dependence obtained corresponds to the known tendency for an increase in q_0 with a decrease in R_∞. In addition, for k = 0.14 the quantity $q_0\sqrt{R_\infty}$ stays constantly above its boundary layer value, and for other k it passes through a minimum, its value there being the more below the boundary layer value the larger the k value. A comparison of the heat flow at the critical point with experimental data is shown in Fig. 8. Here q_0^* is the heat flow referred to that calculated from the Fay-Riddell [4] formula under the assumption that

$$L = 1, \quad K = (\rho_w \mu_w / \rho_s \mu_s)_{0.1} = 1$$

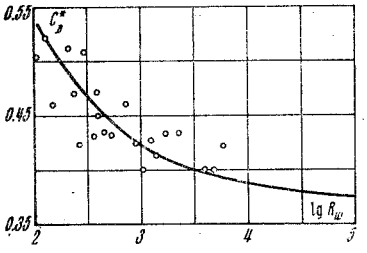

Fig. 11

where L is the Lewis number. The solid curve presents results of our paper (k = 0.35), the dashed curve the results obtained from the formula

$$q_0^* = 1 + 0.52/\sqrt{R_s} \tag{3.3}$$

proposed in [5] on the basis of a treatment of the experimental data ($M_\infty = 6$, $\gamma = 1.4$, $k = 0.33$, $20 \leq R_S \leq 500$). The divergence of the results is obtained within the experimental error limits (7%) indicated by the authors of [5]. The shaded region covers the experimental data given in [6]. For large Reynolds numbers the difference of q_0^* from unity is explained partly by the fact that in using the Fay–Riddell formula, it was assumed that K = 1, whereas for the conditions considered K = 1.064.

Figure 9 shows the distribution over the spherical surface of the reduced heat flow and of the quantity $C_f\sqrt{R_\infty}$ for k = 0.35. Curves 1, 2, and 3 correspond to R_∞ values of 177.5, 3550, and 71,000, respectively; curves 1', 2', 3', and 4' are for R_∞ values of 100, 355, 3550, and 71,000, respectively. It is evident that the distribution of q/q_0 depends on the Reynolds number, tending towards its boundary layer value (dashed curve) as the Reynolds number increases. The substantial difference of the curves $q/q_0(\theta)$ with respect to the Reynolds number holds for large θ, where the heat flow is small. Therefore in the experiments [5], the data of which, with its attendant scatter, is shown by the circled points, no dependence of the distribution of the reduced heat flow on the Reynolds number was observed. The distribution of the friction coefficient also proves to be dependent on R_∞, wherein the maximum value of $C_f\sqrt{R_\infty}$ changes nonmonotonically with a change in R_∞. The boundary layer curve for $C_f\sqrt{R_\infty}$ coincides with the curve 4'. The calculations also showed that for all Reynolds numbers the distributions over the spherical surface of the reduced heat flow and the friction coefficient also depend on the temperature factor.

The distribution of the pressure, referred to the pressure at the critical point, is shown in Fig. 10. Curves 1 and 2 correspond to R_∞ values of 177.5 and 35,500, respectively, for k = 0.7; curve 3 is for R_∞ = 177.5 for k = 0.14. The dashed curve was drawn on the basis of the results obtained from nonviscous flow calculations. It is evident that the viscosity and thermal conductivity of the gas lead to an increase in the reduced pressure. As R_∞ increases, the curves $p_w/p_{w0}(\theta)$ approach the pressure distribution for a nonviscous gas. For a fixed value of the Reynolds number (curves 1 and 3), the reduced pressure distribution differs less from the nonviscous gas case the lower the surface temperature. Figure 11 shows, for k = 0.35, the dependence of the resistance coefficient of the sphere on the Reynolds number R_w. The dimensionless resistance coefficient C_d^* is defined as the ratio of the quantity

$$C_d = 4\,\frac{2(\gamma-1)^{-1} + M_\infty^2}{M_\infty^2}\int_0^{\theta^*}(p_w\cos\theta + {}^1/_2 C_f\sin\theta)\sin\theta\,d\theta \tag{3.4}$$

to the value of the resistance coefficient for free-molecular flow for the case of a purely diffuse reflection [7]. The circled points correspond to the experimental data given in [6].

The authors thank Yu. P. Lun'kin for useful discussions of their work.

LITERATURE CITED

1. A. N. Lyubimov and V. V. Rusanov, Gas Flows around Blunt Bodies [in Russian], Nauka, Moscow (1970), Parts and 2.
2. B. M. Pavlov, "Calculation of the supersonic flow around a cooled sphere on the basis of the complete Navier–Stokes equations," in: Calculational Methods and Programming [in Russian], No. 15, Izd. MGU, Moscow (1970), pp. 19-30.
3. V. V. Shchennikov, "Calculation of the laminar boundary layer along a generator of a sublimating body of revolution," Zh. Vychisl. Matem. i Matem. Fiz., 5, No. 1 (1965).
4. D. Fay and F. Riddell, "Theoretical analysis of heat transfer at the forward critical point washed over by dissociated air," in: Gas Dynamics and Heat Transfer in the Presence of Chemical Reactions [Russian translation], Izd. Inostr. Lit., Moscow (1962), pp. 190-224.
5. R. S. Hickman and W. H. Giedt, "Heat transfer to a hemisphere-cylinder at low Reynolds number," AIAA Journal, 1, No. 3 (1963).
6. J. L. Potter, "The transitional rarefied flow regime," in: Rarefied Gas Dynamics, C. L. Brundin (editor), Academic Press, New York (1967), Vol. 2.
7. W. D. Hayes and R. F. Probstein, Hypersonic Flow Theory, Academic Press, New York (1959).